



Butterfly eyespots evolved via cooption of an ancestral gene-regulatory network that also patterns antennae, legs, and wings

Suriya Narayanan Murugesan^{a,1,2}, Heidi Connahs^{a,1,2}, Yuji Matsuoka^{a,2}, Mainak Das Gupta^a, Galen J. L. Tiong^a, Manizah Huq^a, V. Gowri^a, Sarah Monroe^a, Kevin D. Deem^b, Thomas Werner^c, Yoshinori Tomoyasu^b, and Antónia Monteiro^{a,d,1}

^aDepartment of Biological Sciences, National University of Singapore, Singapore, 117543; ^bDepartment of Biology, Miami University, Oxford, OH 45056; ^cDepartment of Biological Sciences, Michigan Technological University, Houghton, MI 49931; and ^dScience Division, Yale-NUS College, Singapore, 138614

Edited by Günter Wagner, Department of Ecology and Evolutionary Biology, Yale University, New Haven, CT; received May 16, 2021; accepted January 5, 2022

Butterfly eyespots are beautiful novel traits with an unknown developmental origin. Here we show that eyespots likely originated via cooption of parts of an ancestral appendage gene-regulatory network (GRN) to novel locations on the wing. Using comparative transcriptome analysis, we show that eyespots cluster most closely with antennae, relative to multiple other tissues. Furthermore, three genes essential for eyespot development, *Distal-less (Dll)*, *spalt (sal)*, and *Antennapedia (Antp)*, share similar regulatory connections as those observed in the antennal GRN. CRISPR knockout of *cis*-regulatory elements (CREs) for *Dll* and *sal* led to the loss of eyespots, antennae, legs, and also wings, demonstrating that these CREs are highly pleiotropic. We conclude that eyespots likely reused an ancient GRN for their development, a network also previously implicated in the development of antennae, legs, and wings.

evolutionary biology | evolutionary developmental biology | genetics

Although the hypothesis of gene-regulatory network (GRN) cooption is a plausible model to explain the origin of morphological novelties (1), there has been limited empirical evidence to show that this mechanism led to the origin of any novel trait. Several hypotheses have been proposed for the origin of butterfly eyespots, a novel morphological trait. These include cooption of the GRNs that also specify legs (2), embryo segmentation (3), wing margin (4), and that regulate wound healing (5). These hypotheses for eyespot GRN origins all rely on similarities of expression of just a few candidate genes observed in eyespots and in the site of activity of the proposed ancestral gene network. To test whether cooption of any of these networks underlies eyespot origins, we focused on the nymphalid butterfly *Bicyclus anynana*, which has served as a model for studying eyespot development (6). Using RNA sequencing (RNA-seq), we examined and compared the larger collection of genes expressed in a forewing eyespot of *B. anynana* with those expressed in these proposed candidate ancestral traits. Additionally, we examined a few other traits, including larval head horns and prolegs, and also pupal eyes and antennae (Fig. 1A).

The Transcriptome Profile Shows Eyespots and Antennae Cluster Together

We first examined which of the sampled tissues shared the most similar gene expression profile to eyespot tissue, as these should cluster closer together (7). Pairwise differential expression (DE) analysis using DESeq2 (8) identified 10,281 DE genes ($\log_{2}FC \geq |2|$ and $\text{padj} \leq 0.001$) among all tissues sampled. Hierarchical clustering of tissues, using DE genes, resulted in eyespots clustering with antennae (Fig. 1C and *SI Appendix, Fig. S1*), but tissues were also clustering according to developmental stage (Fig. 1B and C and *SI Appendix, Fig. S1*). To circumvent the strong

developmental stage signal, we reanalyzed DE genes solely from 3-h-old pupae, when the eyespot tissue was dissected, using 3-h embryos as an outgroup. We found 7,133 DE genes between the tissues, with eyespots clustering with antennae, and both forming a sister clade to the remaining pupal tissues with a high approximately unbiased (AU) *P* value (9) (Fig. 1D).

To confirm this clustering, we also performed a principal component analysis (PCA) and Spearman correlation analysis between the tissues at 3-h pupal stage. This highlighted that the tissue groups are distinct from each other in multidimensional space and showed eyespots clustering closer to whole wings than to antennae. However, the correlation matrix showed little variation in gene expression between tissues (*SI Appendix, Fig. S2 A and B*), suggesting the distinction between the tissues could be a result of a small subset of genes.

To more narrowly identify the subset of genes associated with eyespot development and to examine similarities in their expression profile with our candidate tissues, we next compared the transcriptome of dissected eyespot tissue with adjoining control tissue in the same wing sector (Fig. 1A), as done by a previous study (10). This previous study identified 183 genes differentially expressed in eyespots relative to sectors of the wing without eyespots. Our new DE analysis between eyespot and control wing tissues identified 652 eyespot-specific DE genes with 370 being up-regulated, which included *sal*, and 282 down-regulated in eyespots (*SI Appendix, Figs. S3 and S4 and Dataset S1*). We mapped the published 183 eyespot DE genes,

Significance

Where do butterfly eyespots come from? One of the long-standing questions in the field of evolution concerns addressing where novel complex traits come from. Here we show that butterfly eyespots, a novel complex trait, likely originated from the redeployment of a preexisting gene-regulatory network regulating antennae, legs, and wings, to novel locations on the wing.

Author contributions: S.N.M., H.C., Y.M., and A.M. designed research; S.N.M., H.C., Y.M., M.D.G., G.J.L.T., M.H., V.G., S.M., and K.D.D. performed research; S.M., H.C., Y.M., and A.M. analyzed data; S.N.M., H.C., Y.M., and A.M. wrote the paper; and T.W. and Y.T. critically revised the manuscript.

The authors declare no competing interest.

This article is a PNAS Direct Submission.

This open access article is distributed under [Creative Commons Attribution-NonCommercial-NoDerivatives License 4.0 \(CC BY-NC-ND\)](https://creativecommons.org/licenses/by-nc-nd/4.0/).

¹To whom correspondence may be addressed. Email: suriya_nm@u.nus.edu, dbshc@nus.edu.sg, or antonia.monteiro@nus.edu.sg.

²S.N.M., H.C., and Y.M. contributed equally to this work.

This article contains supporting information online at <http://www.pnas.org/lookup/suppl/doi:10.1073/pnas.2108661119/-DCSupplemental>.

Published February 15, 2022.

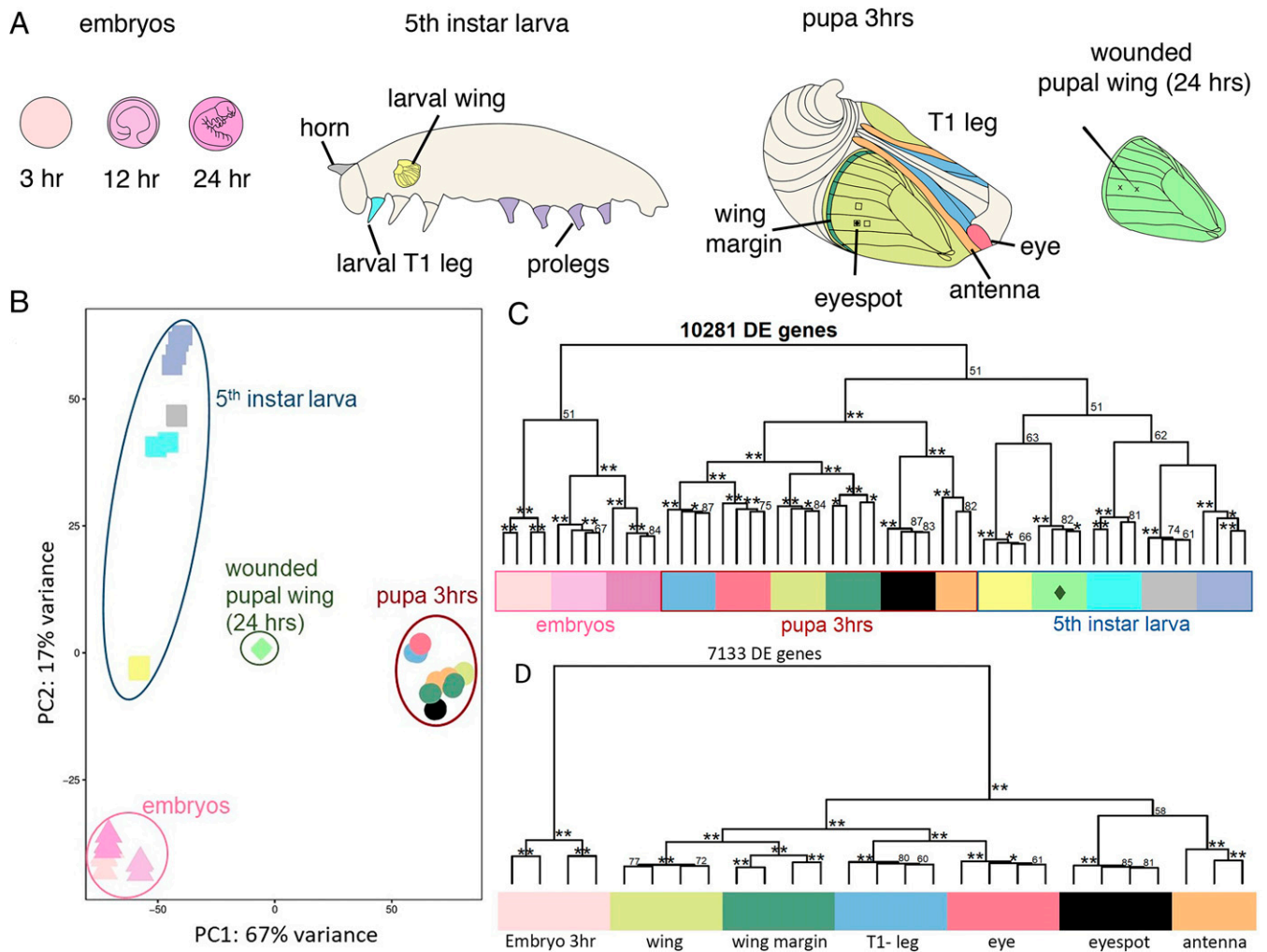


Fig. 1. Tissues used for RNA-seq analysis and character tree constructed using DE genes. (A) We used 16 tissue groups from three separate developmental stages of *B. anynana* for RNA extractions. Embryos at 3 h, 12 h, and 24 h after egg laying. Larval forewings, T1 legs, horns, and prolegs. Pupal antennae, T1 legs, forewings, eyes, wing margins, eyespots, and two eyespot control tissues, all dissected at 3 h after pupation, and a wounded wing dissected at 24 h after pupation. (B) PCA using 10,281 DE genes obtained from pairwise comparisons between different tissues. Tissues are clustered according to their developmental stages. (C) Character tree constructed using 10,281 DE genes showed eyespot tissue clustered with antenna tissue first, and next with tissues from the same developmental stage, except for a 24-h pupal wounded wing (◆), which clustered with larval wing tissue. (D) Character tree constructed using 7,133 DE genes from 3-h pupal stage with 3-h embryos as outgroup showed eyespot tissue clustered with antenna tissue. **100 unbiased (AU) *P* value; *90 to 99 unbiased (AU) *P* value.

which included *Dll* and *Antp*, to the current assembled transcriptome. After removing multimapped genes, we retained 144 genes from the published study for further analysis (Dataset S1). When hierarchical clustering was performed, using either the newly identified 652 genes, the 144 genes previously identified, or both datasets combined, we found that the eyespot transcriptome always clustered with antennae with strong support AU *P* value for the clade. This clustering persisted with just the 370 up-regulated genes (SI Appendix, Fig. S5 A, E, and F).

Given the importance of transcription factors (TFs) in development and in establishing GRNs, we used 336 genes annotated as having “DNA-binding transcription factor activity (gene ontology [GO]:0003700)” and “transcription factor binding (GO:0008134)” in a separate analysis, which showed eyespots again clustering with antennae (SI Appendix, Fig. S5B). Annotation and gene enrichment for the DE genes between the 3-h pupal stage tissues showed a strong enrichment in animal organ morphogenesis (GO:0009887) and anatomical structure formation (GO:2000026) (SI Appendix, Fig. S6). Performing the

clustering analysis using genes from these two groups (GO:0009887 and GO:2000026), in two separate analyses, reproduced the same results as the full gene set, indicating that these morphogenesis genes show similar expression profiles in both eyespots and antennae (SI Appendix, Fig. S5 C and D).

To verify that the square of dissected eyespot tissue has a different transcriptome from those of the other dissected wing tissues, including the Nes1 and Nes2 squares of control wing tissues of the same size (SI Appendix, Fig. S3A), we redid the clustering analysis for the pupal tissue, where we included these two control tissues. The Nes2 piece of wing just anterior to the Cu1 eyespot, in the M3 sector, clustered with eyespot tissue and with antennae. However, Nes1, positioned more proximally to the body in the Cu1 sector, clustered with the wing margin and then with the whole wing (SI Appendix, Fig. S7). This analysis shows that the exact *x-y* coordinates of these pieces of wing tissue contain important positional information. The Nes2 piece of tissue differentiates an eyespot center earlier in the larval stage (Fig. 2 E–M), but several marker proteins, including *Dll* and *Sal*, disappear from these cells by the end of the larval stage (11).

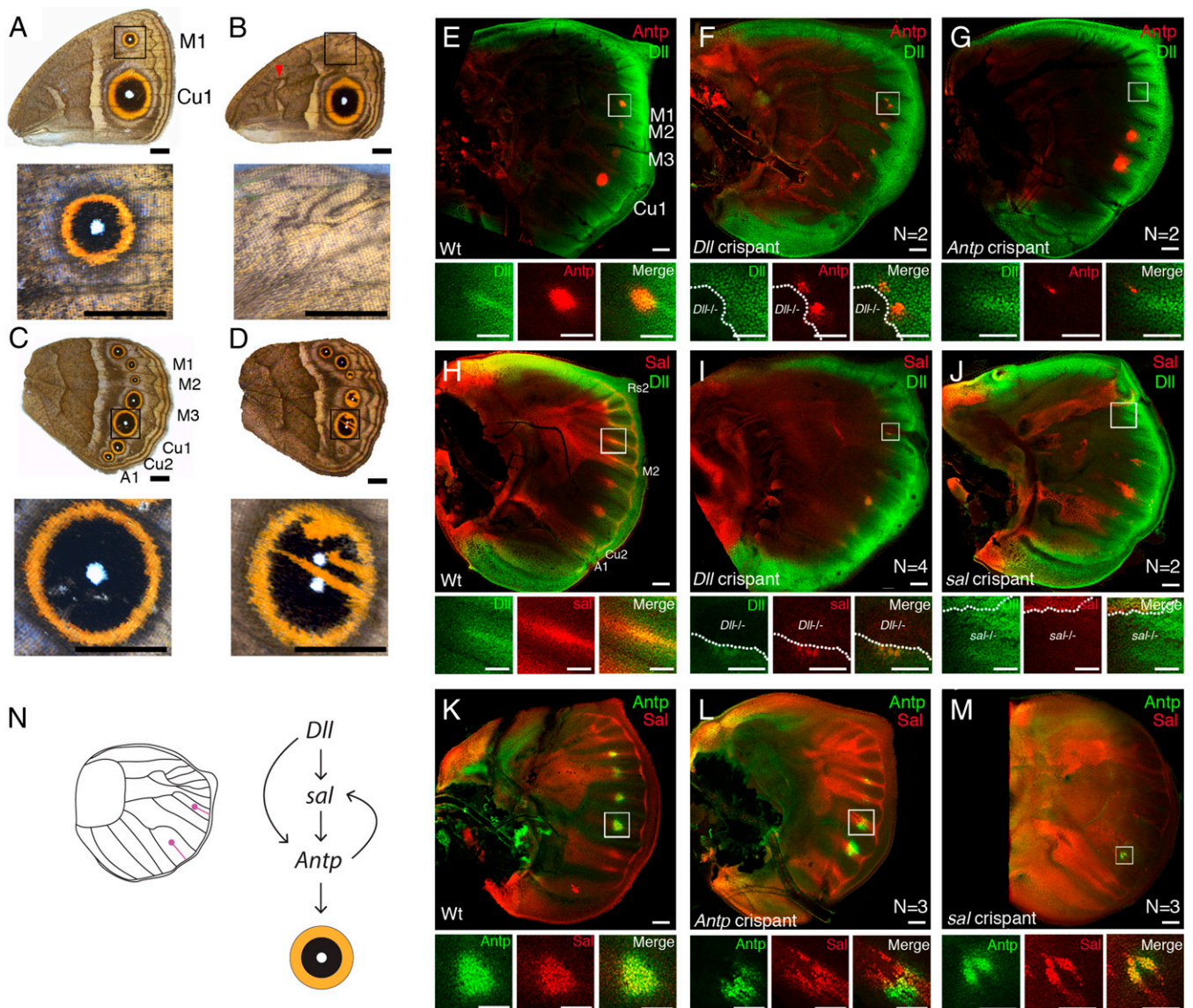


Fig. 2. Function of *sal* and regulatory interactions between *Dll*, *sal*, and *Antp* inferred with CRISPR and immunohistochemistry (A). WT female forewing. (B) *sal* crisprant female forewing. (C) WT female hindwing. (D) *sal* crisprant female hindwing. (E) Levels of Dll and Antp proteins in WT forewing. (F) Levels of Dll and Antp proteins in *Dll* crisprant forewing. (G) Levels of Dll and Antp proteins in an *Antp* crisprant forewing. (H) Levels of Dll and Sal proteins in WT forewing. (I) Levels of Dll and Sal proteins in *Dll* crisprant forewing. (J) Levels of Dll and Sal proteins in *sal* crisprant forewing. (K) Levels of Sal and Antp proteins in WT forewing. (L) Levels of Sal and Antp proteins in *Antp* crisprant forewing. (M) Levels of Sal and Antp proteins in *sal* crisprant forewing. White square regions were highly magnified. (N) Schematic diagram of genetic interaction among *Dll*, *sal*, and *Antp* in the eyespot region of a developing forewing. (Scale bars in A–D: 5 mm for whole wings and wing details.) (Scale bars in E–M: 100 μ m in low and 50 μ m in high magnification.)

However, it is interesting to observe that this tissue still contains a transcriptome that more closely resembles eyespots (and antennae) than any other piece of tissue dissected out of a 3-h-old pupa.

These analyses showed that eyespots and antennae form a sister clade to the other tissues, including legs, which are considered serial homologs to antennae. However, eyespots express a key selector gene, *Antp*, which is known to give legs their unique identity and differentiate them from antennae. *Antp* protein is known to positively regulate *Dll* and repress *sal* in the leg disk of *Drosophila* (12, 13), whereas in the antennae, in the absence of *Antp*, *Dll* activates *sal* (14). Comparative data across 23 butterfly species suggested that eyespots originated without *Antp* protein expression, and that *Antp* was recruited later to the eyespot GRN in at least two separate lineages, including in the ancestors of *B. anynana* (15). We therefore

reasoned that if eyespots are sharing more transcriptome similarities with antennae, rather than with legs, the regulatory interactions between *Dll*, *Sal*, and *Antp* in eyespots should resemble those in insect antennae but not those in legs, and that the regulatory interactions between *Antp* and the other two genes should be novel and not homologous.

Function of *sal* and Regulatory Interactions between *Dll*, *sal*, and *Antp* in Eyespots

Before establishing regulatory interactions between the three genes, we first obtained missing functional data for one of these genes, *sal*, lacking for *B. anynana*. Mutations for *Dll* and *Antp* were previously shown to remove eyespots, pointing to these genes as necessary for eyespot development (6, 16). We disrupted the function of *sal*, using CRISPR with a single guide

RNA (sgRNA) targeting exon 2 (*SI Appendix, Fig. S8*). *sal* crispants (mosaic mutants) showed a range of phenotypes, from missing eyespots (Fig. 2 *B* and *D* and *SI Appendix, Fig. S9*) to altered chevron patterns on the wing margin and the central symmetry system bands running the length of each wing (Fig. 2*B*), all mapping to patterns of *sal* expression in larval and pupal wings (Fig. 2 *H* and *K*) (5, 17). Our data confirmed phenotypes previously shown in *Junonia coenia* (18). However, two novel and striking phenotypes were the splitting of eyespot centers into two smaller centers (Fig. 2*D* and *SI Appendix, Fig. S9*), and the partial loss of black scales in the eyespot and their replacement with orange scales (Fig. 2*D*), resembling the “goldeneye” phenotype (19). Taken together, these results confirm that *sal* is necessary for the development of eyespots, and also for the development of black scales.

To test the regulatory hierarchy between these three eyespot-essential genes, we knocked out each gene in turn, using CRISPR-Cas9, and reared the mosaic individuals until the late fifth instar for larval wing dissections. We performed immunohistochemistry on these wings with antibodies against the protein of the targeted gene and against the other two proteins. We first examined the interaction of *Dll* with *Antp*. In wild-type (WT) wings, Dll protein is present along the wing margin and in finger-like patterns, spreading from the wing margin to the future eyespot centers (Fig. 2*E*), whereas Antp protein is initially present in the center of four putative eyespots (from M1 to Cu1) (20). In a *Dll* crispant forewing, Antp protein levels were affected in *Dll* null cells (Fig. 2*F* and *SI Appendix, Fig. S10*), whereas Dll protein levels were not affected in *Antp* null cells in an *Antp* crispant (Fig. 2*G* and *SI Appendix, Fig. S11*). These results suggest that *Dll* is upstream of *Antp* in eyespot development. We next examined the interaction of *Dll* with *sal*. In WT wings, Sal protein is broadly present along several wing sectors, connected to its role in vein patterning (17), and also present in nine potential eyespot centers (Fig. 2 *H* and *K*). In *Dll* crispants, Sal protein was lost in *Dll* null clones in the eyespot centers (Fig. 2*I* and *SI Appendix, Fig. S12*), but Dll protein levels were not affected in *sal* null clones in *sal* crispants (Fig. 2*J* and *SI Appendix, Fig. S13*). These results suggest that *Dll* is also upstream of *sal* in eyespots. Finally, we examined the interaction between *Antp* and *sal*. In *Antp* crispants, Sal protein is missing from *Antp* null cells (Fig. 2*L* and *SI Appendix, Fig. S14*). Furthermore, Antp protein is missing from *sal* null cells in *sal* crispants (Fig. 2*M* and *SI Appendix, Fig. S15*). Taken together, *Dll* is up-regulating both *Antp* and *sal*, and *Antp* and *sal* are up-regulating each other's expression in forewing eyespots (Fig. 2*N*).

Regulatory Connections between *Dll* and *sal* in Eyespot Development Are Similar to Those in the Antennae of Flies

We next examined whether the appendage expression and regulatory connections between these three genes of *B. anynana* matched those known in fly leg and antennal development. In flies, Dll protein is present in both appendages (21), whereas Sal is only present in antennae and Antp only in legs of flies (14). In *B. anynana*, we observed similar protein profiles in antennae and thoracic legs of pupae (*SI Appendix, Figs. S16 and S17*). Dll is necessary for *sal* expression in antennae of flies (14), as also observed in *B. anynana* eyespots (Fig. 2*L*). Antp, however, negatively regulates *sal* expression in fly legs (13), which differs from the regulation observed in eyespots where *Antp* and *sal* up-regulate each other (Fig. 2*N*). The genetic interaction of *Antp* and *Dll* during leg development in *Drosophila* is stage dependent. At the stage when leg primordia are formed, Antp positively regulates *Dll* expression in the thoracic leg bud (12), but when leg segments are being formed, Dll negatively regulates *Antp* in the distal leg elements (22). These

regulatory interactions between *Dll* and *Antp* in leg development are distinct from the regulatory interaction observed in eyespots (Fig. 2*N*). Taken together, these data suggest that the regulatory interactions between *Dll* and *sal* in eyespots are likely homologous to those in the insect antenna GRN. *Antp* established a novel regulatory interaction to these two genes in eyespots, distinct from those found in the leg context of *Drosophila*. This supports the later and independent addition of *Antp* to the eyespot GRN in two separate lineages of butterflies, as proposed by Oliver et al. (15).

Two Pleiotropic CREs Reveal a Shared Network between Eyespots, Antennae, Legs, Wings, and Other Traits

Evidence of GRN cooption is bolstered by the identification of shared *cis*-regulatory elements (CREs) driving the expression of genes common to both the ancestral and the novel trait (eyespots) (23). To identify putative CREs specific to wing tissue with eyespots, we used formaldehyde-assisted isolation of regulatory elements using sequencing (FAIRE-seq) to identify the open-chromatin profile around *Dll* in forewing and hindwing pupal tissues of *B. anynana*. We produced separate libraries from the proximal and distal regions of the wing, the latter containing the eyespots. Mapping of FAIRE-seq reads from each wing region to a previously published *Dll* bacterial artificial chromosome (BAC) (scaffold length of 230 kb) revealed 18 regions of open chromatin across this scaffold, representing candidate CREs (Fig. 3*A*). A Basic Local Alignment Search Tool (BLAST) search of each candidate CRE against the *B. anynana* genome revealed that most of these regions contained repetitive elements. However, one candidate CRE that was open in the distal forewing at scaffold position 150 kb (Fig. 3*B*) (*Dll319* CRE), returned a unique BLAST hit to the genome. As this region did not contain any repetitive elements, we used CRISPR-Cas9 to disrupt its function. We designed four guide RNAs along its 319-bp length to maximize the likelihood of its disruption (Fig. 3*A* and *SI Appendix, Fig. S18*). We obtained a variety of different phenotypes that were also observed when targeting exons of the *Dll* gene using CRISPR (6): Several caterpillars showed a missing or necrotic thoracic leg (Fig. 3*C* and *SI Appendix, Fig. S19*); adults were missing legs and even a hindwing (Fig. 3*D* and *E*); adults lacked eyespots (Fig. 3*F* and *G*); and adults showed truncated antennae, pigmentation defects, and loss of wing scales (Fig. 3*H* and *SI Appendix, Figs. S19–S22 and Table S1*), all having deletions within the CRE of various sizes (*SI Appendix, Fig. S19*). These findings confirm that the *Dll319* CRE is pleiotropic and further suggest that eyespots use the same GRN as antennae, legs, and wings.

In order to confirm that the *Dll319* contains a functional and pleiotropic CRE, we cloned a 917-bp region containing this CRE into a *piggyBac*-based reporter construct (24) and evaluated its CRE activity in transgenic butterflies. We observed that embryos expressed the reporter gene (EGFP) in antennae, mouthparts, as well as thoracic limbs (Fig. 3*K* and *SI Appendix, Fig. S23*). Later in development we observed EGFP expression in larval and pupal eyespot centers, indicating that this CRE is sufficient to drive gene expression in all these traits (Fig. 3*I* and *J* and *SI Appendix, Fig. S23*). Using this same cloned region containing the *Dll319* CRE, we also observed pleiotropic CRE activity in antennae, mouthparts, legs, and genitalia, when tested in a cross-species setting with *Drosophila melanogaster* (*SI Appendix, Fig. S24*), suggesting that this region contains an ancestral and pleiotropic CRE present in the ancestors of flies and butterflies.

In order to investigate the extent to which other genes of the eyespot GRN share the same open-chromatin profiles as genes expressed in antennae and in other tissues, we performed an assay for transposase-accessible chromatin using sequencing

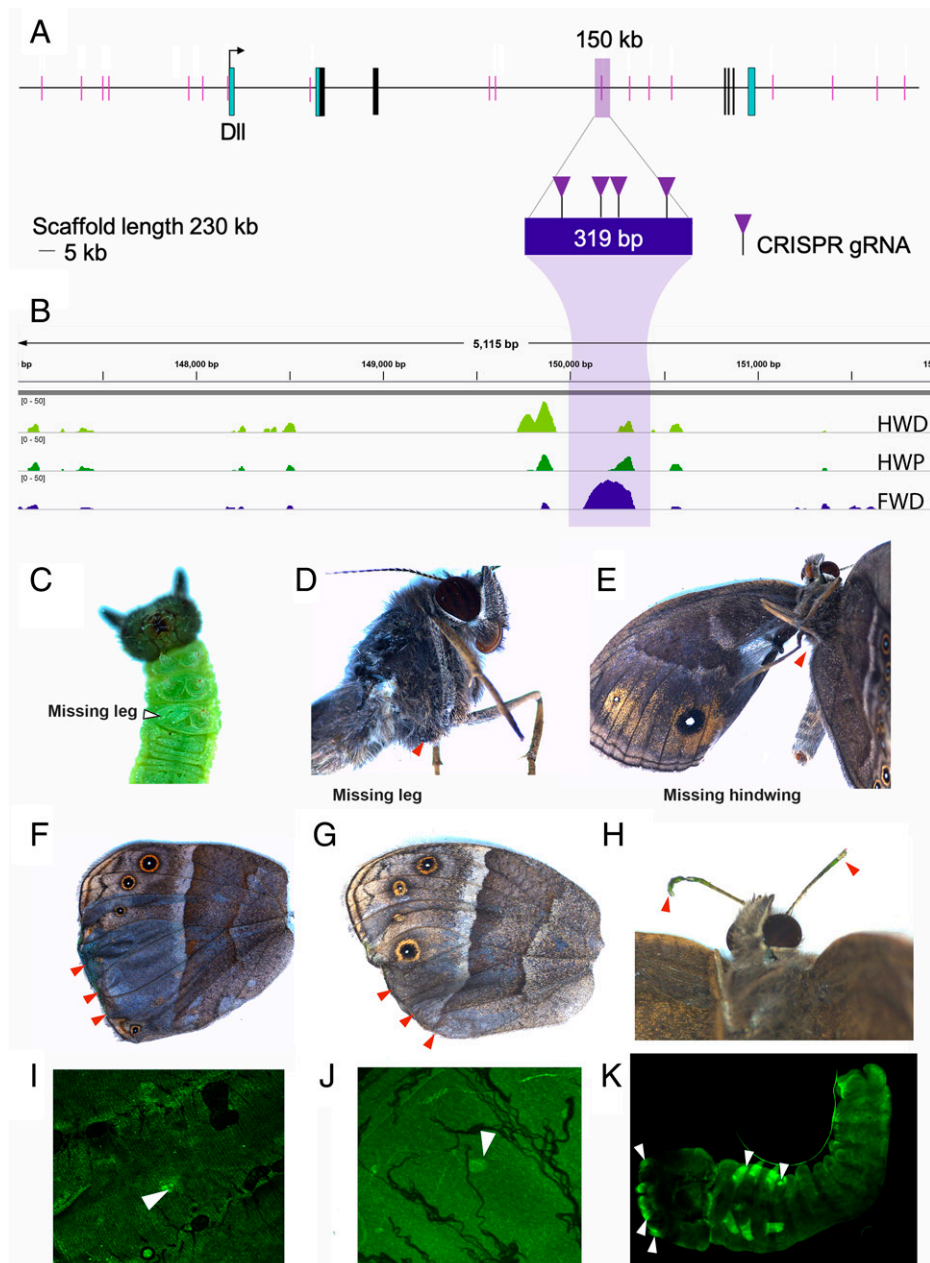


Fig. 3. Multiple traits are affected by disruptions of a single *Distal-less* CRE. (A) *B. anynana* *Dll* locus (previously cloned into a BAC) visualized using IGV showing all 18 FAIRE-seq open-chromatin regions at 24 h postpupation (short pink lines). First exon (untranslated region [UTR] in blue) shows the open-chromatin region (highlighted by a short pink line) at position 54 kb at the transcriptional start site of *Dll*. The FAIRE peak at position 150 kb (*DII319*; highlighted with a purple bar) is open in the *B. anynana* forewing and was targeted with CRISPR. Four RNA guides were used simultaneously to target this region. (B) FAIRE-seq results showing an open region of chromatin in the distal forewing (FWD) at position 150 kb on the *Dll* BAC (blue peak). (C–E) Crispant phenotypes from the same individual: With a missing thoracic leg as a caterpillar, and the same missing thoracic leg, and also missing hindwing, as an adult. (F and G) Crispant wing phenotypes showing loss of eyespots and pigmentation defects. (H) Crispants showing antennal defects. (I and J) *DII319* CRE driving EGFP in eyespot centers in a 24-h pupal wing and a fifth instar larval wing, respectively, in transgenic animals. (K) Transgenic embryo showing EGFP expression driven by the *DII319* CRE in mouthparts, antennae, legs, and pleuropodia (white arrows from *Left* to *Right*). HWD, distal hindwing; HWP, proximal hindwing.

(ATAC-seq) with the same tissues used for the transcriptome analysis. Spearman correlation analysis between the tissues at 3-h pupal stage, using all the open-chromatin regions from the ATAC-seq dataset, highlighted eyespots showing a strong correlation (≥ 0.9) with antennae and wing margin, consistently across all replicates (*SI Appendix, Fig. S25*). A differential accessibility analysis for the open-chromatin regions associated with the eyespot DE genes showed that eyespots shared the greatest number of open-chromatin regions with antennae, as compared to other tissues at the 3-h pupal stage (Fig. 4 G and H).

The ATAC-seq data also showed that the *DII319* CRE is open across all different stages and tissues, irrespective of the expression of *Dll* (Fig. 4A), suggesting that pleiotropic CREs may always be open throughout development. To test this idea, we further targeted a genomic region of *sal* (*sal740*) that had open chromatin across most developmental stages using CRISPR-Cas9 (Fig. 4B). We obtained aberrations in caterpillar horns, adult antennae, legs, and chevron patterns, as well as missing eyespots and a missing wing (Fig. 4 C–F and *SI Appendix, Fig. S26*), again confirming the presence of a pleiotropic CRE for a

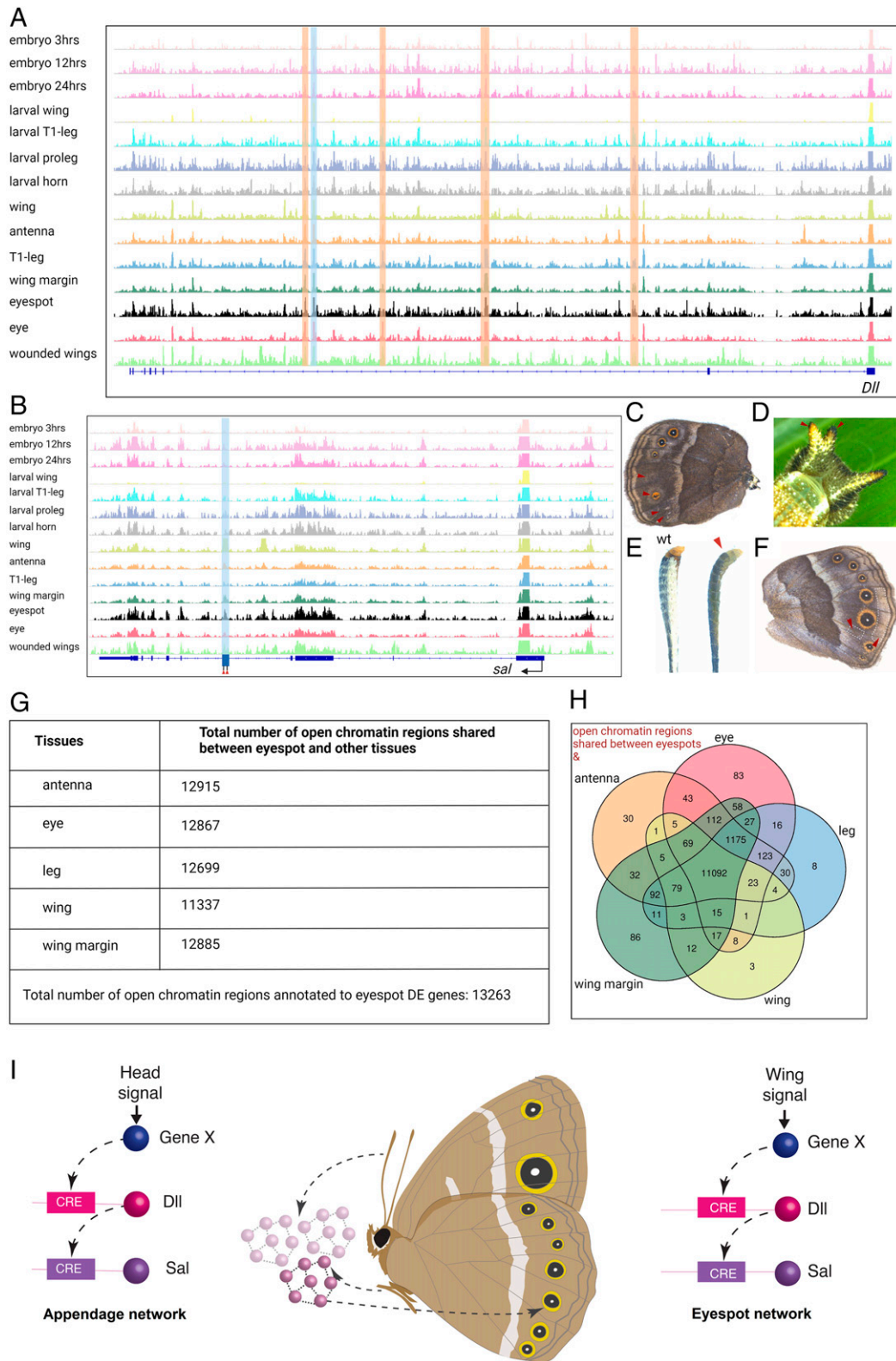


Fig. 4. Visualization of open chromatin around *Dll* and *sal* genomic regions for different tissues, and identification of a *sal* pleiotropic CRE. (A) ATAC-seq reads around the *Dll* genomic region with highlights in the open regions shared across different tissues (orange) and the targeted *Dll319* (blue). (B) ATAC peak regions around the *sal* genomic region with the *sal740*-targeted region highlighted in blue. (C–F) *sal740* crispant phenotypes: Missing and reduced eyespots (C), split horn (D), thinner and discolored antenna compared to wild type (E), lost chevrons in the wing margin and ectopic vein in the Cu2 sector (F). (G) Table with the total number of open peaks associated with eyespot DE genes and number of peaks shared between eyespots and different tissues. (H) Venn diagram showing the number of open-chromatin regions shared between different tissue groups. (I) Schematic illustrating the hypothesis that eyespots evolved via cooption of an ancestral appendage GRN with genes (*Dll* and *sal*) in the GRN reusing the same CREs in both appendages and eyespot development.

gene common to eyespots, antennae, legs, and wings. Overall, fewer crispants were produced when targeting the CREs compared to the coding region of both *Dll* and *sal* genes, likely because coding regions can be more easily disrupted to produce a phenotype compared to CREs (*SI Appendix, Tables S3 and S4*).

To further confirm that the two CREs (*Dll319* and *sal740*) drive *Dll* and *sal* in an endogenous context, we reanalyzed Hi-C data from the wandering larval stage, when Dll and Sal proteins are present in eyespot centers (Fig. 2). Using the *Dll319* and *sal740* CREs as a bait, we observed that these two sequences physically interact with the *Dll* and *sal* promoters, respectively (*SI Appendix, Fig. S27*).

By exploring the gene expression profile and functional regulatory connections of essential genes of the eyespot GRN, we showed that eyespots, a morphological novelty in nymphalid butterflies, likely evolved via cooption of parts of an ancient GRN, that also patterns antennae, legs, and wings. This network, initially deployed in primitive sensory systems in the region of the head, has been subsequently recruited and modified to produce legs (25) and perhaps even wings (26, 27). We showed that the transcriptome profile of eyespots more closely resembles that of antennae compared to any other tested appendage or butterfly tissue. Furthermore, genes known to be critical for eyespot development share the same functional connections as observed in *Drosophila* antennae. Finally, disruptions to CREs of two genes shared between eyespots, legs, and antennae, affected the development of all these traits. Previous studies in *Drosophila* had demonstrated the same CREs driving reporter gene expression in separate traits (1) and CRE disruptions leading to pleiotropic effects on patterns of CRE activity (28). However, here we show that disruptions to two pleiotropic CREs result in the loss of both ancestral and derived traits, which provides strong evidence for GRN cooption.

Future work should examine what proportion of the ancestral appendage GRN was indeed coopted to eyespot development. Our RNA-seq experiment identified hundreds of genes with shared expression profiles between eyespots and antennae but also hundreds more with distinct expression profiles. It is also unclear why eyespots do not grow out of the plane of the wing, as in the case of ventral appendages. It is possible that wing-specific proteins repress such outgrowth, or that only a core set of genes was recruited and rewired to novel downstream genes to produce the unique eyespots.

The *cis*-regulatory paradigm (29) suggests that when a gene is expressed in a different developmental context it uses a different CRE for its activation. Here we show that this does not apply to traits that emerge through gene-network cooption, as the recruited network genes are most likely sharing preexistent regulatory connections (23, 28) (Fig. 4I). The origin of novelties has remained an important unanswered question in biology; and here we show that novelties can arise from GRN cooption, which provides a mechanism for complex traits to evolve rapidly from preexisting traits.

Materials and Methods

Butterfly Husbandry. *B. anynana* were maintained in laboratory populations and reared at 27°C and 60% humidity inside a climate room with a 12:12-h light:dark cycle. All larvae were supplied with young corn leaves to complete their development until pupation. Following pupation, the pupae were collected and placed in a separate cage until they emerged. The butterflies were fed every other day with banana on moist cotton in Petri dishes.

Wing Library Preparation and FAIRE-Seq Analysis. Wings were dissected from *B. anynana* at ~22 to 26 h postpupation. For control input libraries (nonenriched), two whole forewings and two whole hindwings were pooled. Three FAIRE-enriched libraries were prepared in total, including a forewing distal library (the pupal wing was cut in half and the distal region was used for the library) and two hindwing libraries, using both the proximal and distal regions of the wing. All FAIRE-enriched libraries were prepared from seven to eight

pooled wing tissues. Libraries were prepared by Genotypic Technology (India) as 75-bp pair-end reads and sequenced using Illumina NextSeq. Raw reads were quality checked and reads with phred scores >30 were retained for downstream analyses. Following the removal of adapters and low-quality bases, the reads were aligned to a *B. anynana* BAC sequence containing *Dll*, with Burrows-Wheeler Aligner (0.7.13) (30), using the following parameters: -k Integer (INT), -w INT, -A INT, -B INT, -O INT, -E INT, -L INT, -U INT. The resulting SAM files were converted to binary alignment map (BAM) files, using SAMtools-0.1.7a (31). The BAM files were converted to sorted BAM, followed by removal of PCR duplicates. The final BAM files were converted to BEDgraph files, using BEDtools-2.14.3 (32). Peaks were called with MACS2 software (33), using the aligned enriched and input (control) files with the q value (minimum false discovery rate [FDR]) cutoff to call significant regions. The command `bdgcmp` script was used on the enriched and input BEDgraph files to generate fold enrichment and log likelihood scores. This command also removed noise from the enriched sample relative to the control. The BEDgraph files were converted to BigWig files for visualization in Integrative Genomic Viewer (IGV).

Identifying CREs for CRISPR-Cas9 Experiments. The FAIRE-seq data were visualized using IGV. All 18 candidate CREs identified around the *Dll* locus were blasted against the *B. anynana* genome in LepBase to verify whether they were unique in the genome. Most of the candidate CREs were not unique and had multiple hits throughout the genome. One of the unique regions, the CRE *Dll319*, was selected as a suitable target for CRISPR knockout.

Single Guide RNA Design and Production. sgRNA target sequences for *sal* were selected based on their GC content (around 60%) and the number of mismatch sequences relative to other sequences in the genome (more than three sites). In addition, we selected target sequences that started with a guanine for subsequent *in vitro* transcription by T7 RNA polymerase. sgRNA for the *Dll319* CRE were designed using CRISPR Direct (34), corresponding to GGN20NGG. We designed four guides spanning the length of the CRE (Fig. 3B and *SI Appendix, Fig. S18 and Table S2*). Two guides were designed targeting the *sal740* region (*SI Appendix, Fig. S28 and Table S2*). The sgRNA templates were created by a PCR with overlapping primers, using Q5 polymerase (New England Biolabs [NEB]). Constructs were transcribed using T7 polymerase and (10×) transcription buffer (New England Biolabs), RNase inhibitor (RiboLock), nucleoside triphosphates (NTPs) (10 mM), and 600 ng of the PCR template. The final sample volume was 40 μL. Samples were incubated for 16 h at 37°C and then treated with 2 μL of DNase 1 at 37°C for 15 min. Samples were purified by ethanol precipitation, and RNA size and integrity were confirmed by gel electrophoresis.

Cas9 mRNA Production. The plasmid pT3TS-nCas9n (Addgene) was linearized with *Xba*I (NEB) and purified by phenol/chloroform purification and ethanol precipitation. pT3TS-nCas9n was a gift from Wenbiao Chen, Vanderbilt University, Nashville, TN (Addgene plasmid #46757; <http://addgene.org/46757>; Research Resource identifiers [RRID]:Addgene_46757). *In vitro* transcription of mRNA was performed using the mMESAGE mMACHINE T3 kit (Ambion). One microgram of linearized plasmid was used as a template, and a poly(A) tail was added to the synthesized mRNA by using the Poly(A) Tailing Kit (Thermo Fisher). The A-tailed RNA was purified by lithium-chloride precipitation and then dissolved in RNase-free water and stored at -80°C. The Cas9 transcript was used for producing *sal* crispants and for the analysis of regulatory interactions among *Dll*, *Antp*, and *sal*.

In Vitro Cleavage Assay for the *Dll319* CRE. The sgRNAs were tested using an *in vitro* cleavage assay. Wild-type genomic DNA was amplified using primers that were at least 200 bp from the sgRNA sites. sgRNA (200 ng/μL per guide), Cas9 protein (800 ng/μL) (stored in a buffer containing 300 mM NaCl, 0.1 mM edetate disodium salt dihydrate, 1 mM dithiothreitol, 10 mM Tris-HCl, 50% glycerol pH 7.4 at 25°C), NEB buffer 3 (1 μL), and bovine serum albumin (BSA) (1 μL) were brought to a final volume of 10 μL with nuclease-free water and incubated at 37°C. After 15 min of incubation, the purified amplicon (100 ng) was added to the sample, which was then incubated for an additional 1 to 2 h at 37°C. The entire reaction volume was analyzed on a 1% agarose gel. Cas9 protein was purchased from NEB EnGen Cas9 nuclear localization sequence. The cleavage assay confirmed that each guide successfully cleaved the PCR amplicon.

Embryo Injections. Wild-type laboratory populations of *B. anynana* adults were provided with corn plants to lay eggs. The eggs were collected within 1.5 h of oviposition and placed onto 1-mm-wide strips of double-sided tape in plastic Petri dishes (90 mm). Cas9 protein (final concentration 800 ng/μL) and sgRNA (final concentration 200 ng/μL per guide) for all four guides were prepared in a total volume of 10 μL and incubated for 15 min at 37°C prior to injection along with 0.5 μL of food dye to improve visualization of the injected

sample into the embryos. For *sal* crispants, Cas9 mRNA (500 µg/µL final concentration) and sgRNA (500 µg/µL final concentration) were injected along with one-tenth of the volume of food dye. For *sal740* CRE, eggs were injected with the mix of Cas9 protein (final concentration 800 ng/µL) and sgRNA (final concentration 400 ng/µL per guide). The injection mixture was kept on ice after the incubation and prior to injection. Embryo injections were carried out by nitrogen-driven injections through glass capillary needles. Injected eggs were stored in closed Petri dishes containing cotton balls that were dampened daily to maintain humidity. The hatched larvae were reared in small paper cups for 1 wk and then moved to corn plants to complete their development. *SI Appendix, Tables S1, S3, and S4* summarize the injection results.

In Vivo Cleavage Assay and Genotyping of *sal* Crispants. Genomic DNA was extracted with a sodium dodecyl sulfate (SDS)-based method from a pool of five injected embryos that did not hatch. About 250 bp of sequence spanning the target sequence was amplified with PCR BIO Taq Mix Red (PCR Biosystems), and PCR conditions were optimized until there were no smears, primer dimers, or extra bands. Primers are listed in *SI Appendix, Table S2*. The PCR products were purified with the GeneJET PCR purification kit (Thermo Fisher). A total of 200 ng of PCR product was denatured and reannealed in 10x NEB2 buffer. One microliter of T7 endonuclease I (NEB) was added to the sample, while 1 µL of MQ water was added to a negative control. Immediately after the incubation for 15 min at 37°C, all the reactions were analyzed on a 3% agarose gel. Amplicons that showed positive cleavage from the T7 endonuclease I assay were subcloned into the pGEM-Teasy vector (Promega) through Thymine and Adenine (TA) cloning. For each target, we picked eight colonies, extracted the plasmid with a traditional alkali-SDS method, and performed a polyethylene glycol (PEG) precipitation. Sequence analysis was performed with the BIGDYE terminator kit and a 3730xl DNA Analyzer (Thermo Fisher).

Screening and Genotyping *Dll319* Crispants. Newly emerged caterpillars were screened under a microscope to look for developmental defects affecting any regions where *Dll* is expressed, such as the thoracic legs, mouthparts, and prolegs. Any caterpillars exhibiting defects were imaged and reared individually in paper cups until the butterflies eclosed. Caterpillars that died were immediately frozen for DNA isolation and genotyping. All other surviving caterpillars with no apparent developmental abnormalities were reared in groups on corn plants and fed ad libitum every 2 d until pupation. The eclosed butterflies were frozen individually at -20°C. Each butterfly was carefully screened under a microscope and examined for asymmetric crispant phenotypes, focusing particularly on phenotypes expected for a *Dll* knockout, such as appendage, eyespot, or pigmentation defects.

Colony PCR to Identify CRE Deletions. For selected crispants, genomic DNA was extracted from the thorax (E.Z.N.A. tissue DNA kit) and used for PCR to prepare samples for genotyping. The samples were visualized on a gel to confirm the correct size band and the PCR product was purified using a Thermo Scientific PCR purification kit. The DNA was cloned into a pGEM T-Easy Vector (Promega) and the plasmid was transformed into DH5 alpha *Escherichia coli*. White colony selection was used for colony PCR. The bands were visualized on a 1% agarose gel to look for bands with shifts relative to the WT band. PCR products from colonies showing evidence of a deletion were submitted for Sanger sequencing PCR (Axil Scientific, Singapore), including a sample that was amplified from *B. anynana* wild-type genomic DNA.

Butterfly Enhancer Reporter Assay. A 917-bp region containing the *Dll319* CRE was cloned into the piggyGUE vector via Gateway technology (Thermo Fisher). piggyGUE is the EGFP version of piggyGUM, the piggyBac-based reporter construct that was previously published (24). The details of piggyGUE will be published elsewhere. The 917-bp region was amplified from *B. anynana* wild-type genomic DNA using a primer containing CACC at the 5' end for directional cloning. The PCR product was cloned into the pENTR vector and further cloned into the piggyGUE vector via a ligation reaction, as described by Lai et al. (24). A total of 4 µL of the LR reaction mix was used for bacterial transformation. After sequence analysis to confirm the presence of SNPs in the *Dll319* CRE, plasmid DNA was amplified, using a Midiprep kit (Qiagen). The piggyGUE *Dll319* CRE plasmid was diluted to 1 µg/µL and mixed in a 1:1 ratio with a hyperactive piggyBac transposase plasmid (35). Embryos ($n = 550$) were collected from *B. anynana* butterflies reared at 27°C and injected ~1 h after egg laying with the plasmid solution and a small amount of food dye, using a glass injection needle and nitrogen gas pressure. Eggs were transferred in a Petri dish to a chamber and kept moist to prevent dehydration. From this batch of eggs, 40 caterpillars hatched and were reared in paper cups during the first week and then transferred to cages with corn plants to complete their development. At all stages, caterpillars were fed corn ad libitum. From this batch of caterpillars, 19 reached adulthood (10 females and 9 males).

These butterflies were evenly distributed into four cages (~5/cage) and placed with respective wild-type males and females for breeding. We were unable to observe any *dsRed* signal (the positive marker of transgenesis driven by the 3xP3 promoter) in the eyes of the caterpillars from the F1 or F2 generation, despite ubiquitous *dsRed* signal in some first instar larvae (only) of the F1 generation, which were used later for outcrossing to wild-type individuals. This ubiquitous signal was not observed again in the offspring of these larvae. We collected eggs from the F3 generation and dissected some embryos for EGFP antibody staining. Two of the four dissected embryos showed expression of EGFP driven by the *Dll319* CRE in the embryonic antennae, mouthparts, thoracic legs, and pleuropodia (Fig. 3K and *SI Appendix, Fig. S23*). Subsequent hemolymph PCR genetic screening in individuals of the fourth generation failed to identify additional positive individuals and the line was lost. A second line was created, using similar methods as described above, where we were able to observe EGFP expression in the eyespot centers at both larval and pupal stages ($n = 6$) and also in embryos ($n = 2$).

Drosophila Enhancer Reporter Assay. The same 917-bp sequence that contained the *Dll319* CRE was directionally cloned into pENTR-D, then Gateway cloned into the piggyPhiGUGd, the Gal4-delta version of the previously reported piggyBac-based reporter construct (24). piggyPhiGUGd also has an attB site, allowing phiC31 transgenesis. For *Drosophila* transgenesis, the piggyPhiGUGd *Dll319* CRE construct was transformed into the attP2 site (68A4) through phiC31 integrase-mediated transgenesis system with EGFP as a visible marker (BestGene *Drosophila* transgenic service). Established transgenic flies were crossed with G-TRACE (36) to visualize the tissues with CRE activities.

Antibody Staining of *B. anynana* Embryos and Wings. Two-day-old embryos, as well as fifth instar larval and pupal wing tissues were dissected in phosphate buffered saline (PBS) buffer under the microscope. The samples were fixed in 4% formaldehyde/fix buffer (0.1 M Pipes pH 6.9, 1 mM ethylene glycol tetraacetic acid pH 6.9, 1.0% Triton X-100, 2 mM MgSO₄) for 30 min on ice. The samples were washed with 0.02% PBSTx (PBS + Triton X-100) three times every 10 min and then blocked in 5% BSA/PBSTx for 1 h. The samples were then incubated in 5% BSA/PBSTx with the primary antibody, and incubated at 4°C overnight. As primary antibodies, we used a rabbit polyclonal anti-Dll (at 1:200, a gift from Grace Boekhoff-Falk, University of Wisconsin, Madison, WI), a mouse monoclonal anti-Antp 4C3 (at 1:200; Developmental Studies Hybridoma Bank), a rabbit anti-Sal (at 1:20,000 for wings and pupal tissues, and 1:2,000 for embryos) (37), and a rabbit anti-EGFP antibody (at 1:200; Abcam ab290) for the transgenic embryos at 24 h ($n = 4$), larval wing discs from the fifth instar ($n = 3$), and pupal wings at 24 h ($n = 3$), as well as WT controls ($n = 2$). For double staining, we added two primary antibodies to the same tube. The wings were washed with PBSTx three times every 10 min. Then, we replaced the PBSTx with 5% BSA/PBSTx to block for 1 h, followed by incubation with the secondary antibody (1:200) in 5% BSA/PBSTx at 4°C for 2 h. The wings were washed with PBSTx three times every 10 min, followed by mounting the wings in ProLong Gold Antifade Mountant (Thermo Fisher). The images were taken under an Olympus FV3000 confocal laser scanning microscope.

Sample Collection and Library Preparation for RNA Sequencing. In order to identify gene expression patterns specific to eyespot formation on the developing wings, we extracted RNA from 16 different tissue types: 3- to 4-h-old, 12- to 13-h-old, and 24- to 25-h-old embryos; T1 legs, prolegs, forewings, and horns from wandering caterpillars; T1 legs, antennae, forewings, forewing margins, eyes, eyespots, and two control tissues adjacent to eyespot centers from 3-h-old pupae (Fig. 1A). For wing wounding experiments, we poked one wing between 17 and 18 h after pupation in two different places in the M3 sector, using a fine tungsten needle with a diameter of 0.25 mm and 0.001 mm at the tip (FST No. 10130-10). We collected the wings 6 h later, which corresponds to 23 to 24 h after pupation, and we also collected the other nonpoked wings as controls (5). In addition, we also collected tissues from 24-h-old and 48-h-old forewings for the clustering analysis. We performed the experiments with four biological replicates for each tissue type with 10 to 25 female individuals in each replicate (both left and right tissues were used, except for the wounded pupal wings, where a single wing was used) (*SI Appendix, Table S5*). Total RNA was extracted in 70 µL of nuclease-free water, using the Qiagen RNA Plus Mini kit. RNA quantity and integrity were measured using a Nanodrop and an RNA bleach gel (38). RNA libraries were prepared using the Truseq stranded mRNA kit from Illumina. Forty million reads were sequenced for each replicate using NovosEq. 6000, with 150-bp paired end and an average insert size of 250 to 300 bp. Library preparation and sequencing were carried out at AIT Novogene, Singapore. In order to avoid batch effects, we randomized the sample extraction and RNA isolation, such that two replicates of the same group were never extracted at the same time.

RNA-Seq Analysis. The raw RNA-seq data were quality controlled and filtered. Adapter sequences and reads with low quality (less than Q30) were trimmed, using bbduk scripts (ktrim = r, k = 23, mink = 11, hdist = 1, tpe, tbo, qtrim = rl, trimq = 30, minlen = 40). In order to remove any bacterial contamination in the samples, we used the bbsplit script, which is a part of the bbmap tools (39). All bacterial genomes were downloaded from the National Center for Biotechnology Information (NCBI) (last downloaded in June 2018), and the reads were mapped to the bacterial genomes, using bbmap. Only reads whose pairs also passed through the filter were further analyzed. To remove any ribosomal RNA sequences from the RNA-seq data, the reads were aligned to the eukaryotic rRNA database available in sortmeRNA (40). The processed reads from different samples were then mapped to the BaGv2 genome, using hisat2 (41) (mapping statistics in *SI Appendix, Table S6*), resulting in bam files that were sorted by genomic positions, using samtools (31). They were used as inputs in StringTie (41) to create the initial transcriptome assembly with 71,042 transcripts, which was used to annotate the genome using Maker v.3 (42), resulting in 18,196 genes with 29,389 transcripts.

RNA-Seq DE Gene Analysis. A read count matrix of the annotated genes was obtained for the samples using StringTie (41). We used the GO terms to filter out any ribosomal genes before obtaining the read counts. This approach led to the removal of 496 genes to a final set of 17,700 genes, which was used throughout the analysis. Correlations between the replicate samples were analyzed using DESeq2 (8) with a sample distance matrix. One of the antennal samples was removed due to its poor correlation with its other biological replicates. The remaining samples were used for the downstream analyses (*SI Appendix, Fig. S29*).

Identifying Eyespot-Specific DE Genes. To identify eyespot-specific genes, a pairwise DE analysis was performed between eyespot and control adjacent tissues, Nes1 and Nes2, using DESeq2 (Fig. 1A and *SI Appendix, Fig. S3*). Common genes up-regulated and down-regulated between eyespot vs. Nes1 and eyespot vs. Nes2 with an adjusted *P* value (padj) of 0.05 were chosen as eyespot-specific DE genes (*Dataset S1*).

RNA Hierarchical Sample Clustering. In order to identify the tissue with the closest gene expression profile to eyespots, we used all tissue samples except the eyespot control tissue samples. DE analysis between the multiple tissues was performed, using run_DE_analysis.pl script provided in Trinity tool, using DESeq2 as the method of choice for this analysis (43). Hierarchical clustering was performed for the different tissues, using genes that showed a log2fold change of $|2|$ and padj value of 0.001, as in Fisher et al. (44). Clustering was performed using an Euclidean distance matrix derived using the DE genes for the tissues with the hclust function in R (45). The pvclust package (9) in R was used to calculate the uncertainty in the hierarchical clustering with a 1,000 bootstrap value. PCA and Spearman correlation analysis for 3-h pupal tissues were carried out using DESeq2 and corplot (46).

ATAC-Seq Library Preparation. We prepared ATAC libraries for the same set of tissues as we did for the RNA-seq experiment, except for the eyespot control tissues (*SI Appendix, Table S7*). Library preparation failed for a few groups leading to two to four biological replicates per group. Tissues were collected, flash frozen in liquid nitrogen, and stored in -80°C , before we extracted nuclei and prepared the libraries. We used 10 to 25 individuals and $\sim 80,000$ nuclei per replicate. Libraries were prepared as described in the Omni-ATAC protocol (47) with slight modifications. Individual tissues extracted at different time periods during the process were randomized and pooled into each replicate before extracting the nuclei. The tissues were thawed and homogenized in 2 mL of ice cold 1 \times homogenization buffer (HB) in a 2-mL glass douncer. Homogenization was performed by 10 strokes with pestle A, followed by 15 strokes with pestle B. The homogenized mixture was left on ice for 2 min before filtering it through a 100- μm nylon mesh filter into a DNA “low bind” 2-mL Eppendorf tube (2666556-250EA). The filtered mixture was centrifuged at 2,500 rpm, and the pellet (the nuclei) was collected along with 50 μL of the solution at the bottom, keeping unwanted cytoplasmic RNAs in the top layers. The filtered nuclei were diluted in ATAC-resuspension buffer (RSB buffer), and 10 μL of the solution was used to count the nuclei, using a hemocytometer. Approximately 80,000 cells were used for each replicate to prepare the libraries. The tagmentation enzyme (TDE1) was obtained from Illumina (Illumina tagment dna tde1 enzyme and buffer smaller kits No. 20034197). As the concentration of the TDE1 and cell number greatly affect the identification of open-chromatin regions, we estimated the amount of enzyme needed for each reaction, using the formula: volume of enzyme = genome size of *B. anynana* [475MB] * number of cells [80,000] * 2.5/(genome size of humans [3200MB] * 50,000). We used 0.65 μL (final concentration of 10.4 nM) of enzyme for each reaction. The Omni-ATAC transposition reaction was carried

out as follows: 80,000 cells suspended in ATAC-RSB buffer were centrifuged at 2,500 rpm for 10 min at 4°C . The supernatant was removed, and the nuclei-containing pellet was kept. To perform the cell lysis, 50 μL of ice-cold ATAC-RSB was added to the pellet, along with 0.1% Nonidet P-40, 0.1% Tween-20, and 0.01% digitonin. The mixture was incubated for 3 min on ice. Subsequently, 1 mL of ATAC-RSB buffer containing only 0.1% Tween and no Nonidet P-40 nor digitonin was added, and the mixture was centrifuged at 2,500 rpm. The supernatant was discarded, and the pellet was retained, to which 50 μL of transposition mixture (6.5 μL 2 \times TD buffer, 0.65 μL transposase (10.4 nM final concentration), 16.5 μL PBS, 0.5 μL 1% digitonin, 0.5 μL 10% Tween-20, 25.35 μL H $_2$ O) was added. The reaction was incubated for 25 min at 37°C at 1,000 rpm in a thermomixer. After the transpositions and tagmentation occurred, the samples were prepared for sequencing by adding Illumina/Nextera adapters with dual indexing and further PCR amplified for 10 cycles. The PCR products were purified, using a Zymo-DNA Clean & Concentrator-5 kit, and the DNA fragments were size selected between 50 and 1,500 bp, using the ProNex Size-Selective Purification System (NG2002) from Promega. The samples were sequenced, using NovosEq. 6000 with an average read depth of 30 million and 2 \times 50 bp paired end reads by AIT Novogene, Singapore.

ATAC-Seq Peak Calling. ATAC-seq analysis was performed as described in Lewis et al. (48) and Lewis and Reed (49) with modification. ATAC reads were processed, using bbduk scripts from bbmap tools to remove any adapters. The reads were mapped to the BaGv2 genome, using bowtie with the $-x$ 1500 and $-m$ 1 parameters. Only reads with insert sizes of 1,500 bp or less and only those mapping to a unique region of the genome were mapped. Reads mapped to the mitochondrial genome were removed, using samtools idxstats, and reads marked for PCR duplicates were also removed, using GATK MarkDuplicates. We kept only paired-end mapped reads with a phred quality score of Q20 and above for downstream analysis. Because the Tn5 transposase binds to DNA as a dimer and inserts adapters of 9 bp in length at the insertion sites, the start sites of the mapped reads were adjusted to an offset of +4 bp in the forward strand and -5 bp in the reverse strand. The bam files were converted to bed files, using Bedtools (32), and we used F-Seq (50) to call peaks for each sample. Bedtools intersect was used to identify the common set of peaks for each tissue type. Peaks from all samples were merged if they were separated by 50 bp, using Bedtools merge to create 313,425 consensus peaks used for the downstream analyses. FeatureCount from the Subread package (51) was used to extract a read count matrix corresponding to the consensus peaks for all samples. The FRiP score, which is defined as the fraction of all reads that are mapped to peaks across the entire genome, was used to measure the quality of the ATAC-seq data. Our ATAC-seq data showed a median FRiP score of 0.846, which is higher than the ENCODE standard (>0.3) for the fraction of reads falling into peaks (*SI Appendix, Table S8*). DeepTools (52) was used to access the sample correlation between the replicates and quality of the libraries (*SI Appendix, Fig. S30*).

ATAC-Seq Differential Peak Analysis. Differential peak analysis was performed using DESeq2 for 3-h pupal tissues. Peaks were considered differentially accessible with a padj value of 0.05. We also mapped the *Dll319* peak identified from the FAIRE data to the BaGv2 genome, using blastn, to identify its position in the new genome assembly and test whether the ATAC-seq analysis was also able to identify it. To identify potential CREs for *sal*, ATAC peaks from 3-h pupal tissues were visualized using IGV and we targeted one potential candidate region (*sal740*) within the intronic region of *sal* gene loci, which is open across almost all of the tissues. Spearman correlation analysis between the 3-h pupal tissues was performed using deepTools (52).

Hi-C Analysis and Virtual 4C. Hi-C analysis was performed as described in Lewis et al. (48). The Hi-C library used for scaffolding the *B. anynana* genome was reanalyzed, using the *Dll319* and *sal740* region as bait, to verify whether these regions interacted with the promoter of *Dll* and *sal*, respectively. Libraries were mapped to the BaGv2 assembly, using Juicer (53). We used the contact map obtained from Juicer to construct a virtual 4C plot for the window around the *Dll319* and *sal740* regions by placing reads in a 3-kb bin, using the script from ref. 54.

Screening and Genotyping *sal740* Crispants. Caterpillars that emerged were carefully screened under the microscope for any defects in their body, especially in the head region where *sal* expression is observed. Individuals showing any abnormalities were imaged and grown separately in a cup, whereas all others were grown in a separate cage. Adults were immediately frozen at -20°C after emergence and screened later under a microscope for any defects in eyespots, wings, legs, and antennae. DNA was extracted from the crispant wing. PCR amplified the target region and amplicon sequencing was done using MisEq. 2 \times 250 bp with 50,000 reads at Genewiz, China.

Hi-C Genome Assembly. Eggs were collected from a single pair of mated *B. anynana* butterflies and reared. Eighteen female siblings were harvested at the wandering stage for DNA extraction. Guts were removed, and the samples were immediately flash frozen in liquid nitrogen and stored at -80°C before the samples were sent to Dovetail Genomics to perform Chicago and Hi-C library preparation and analysis. The Chicago library preparation uses in vitro chromatin fixation, digestion, and cross-linking of regions in the genome that are close to each other in terms of three-dimensional (3D) chromatin architecture. In order to sort and scaffold the genome, 233 million reads (2×150 bp) were sequenced from the Chicago library and mapped to the previously published *B. anynana* genome (v1.2) with 10,800 scaffolds (55). The HiRise pipeline was used to identify misassemblies, to break the scaffolds, and to sort the scaffolds. Only scaffolds greater than 1 kb in length ($n = 5,027$) were used because scaffolds needed to be long enough for the read pairs to align and be scaffolded in accordance with the likelihood model used by HiRise. Next, 153 million reads (2×150) sequenced from the Hi-C library were mapped to the genome assembly output generated from the Chicago-HiRise pipeline to identify any misassemblies from the Chicago pipeline and correct them to produce a final genome assembly of high contiguity.

The genome assembly obtained from the HiC pipeline was ordered, using the available linkage information from Beldade et al. (56), using Chromonomer (57). A total of 289 SNP FASTA sequences were mapped to the Hi-C assembly, using blastn to identify their corresponding positions in the Hi-C genome. Using the SNP position obtained from blastn, a list describing the genetic map was manually created, which later passed through Chromonomer to sort the Hi-C assembly resulting in the final assembly (BaGv2) that was used for the current study. The BUSCO score (58) was used to check for the completeness of the gene sets in the assembly.

Genome Annotation. The genome was repeat masked for transposable elements, small repeats, and tandem repeats before annotation as described in ref. 55. The soft repeat-masked genome was annotated, using four rounds of Maker v.3 (42). The transcriptome assembled from the RNA-seq data and gene sequences annotated from the previous version of the genome were combined and used as transcripts for the species, with transcriptome and protein

sequences from *Pieris rapi*, *J. coenia*, and *Bombyx mori* as relative transcripts and protein homology evidences for the first round of gene predictions. Output gene predictions from each round were used as input for the next round. Snap and Augustus were used for the second round of gene predictions, followed by Genemark for the third round of gene modeling. Then we performed one final round of Snap and Augustus predictions. The minimum length of 35 amino acids was set for gene predictions. The predicted gene models were kept for genes that had an annotation edit distance (AED) score of <1 and/or had a gene ontology obtained from Interproscan (59). This resulted in 18,189 genes with 29,490 transcripts. In order to correct the annotations and produce a standardized gff3 file, the gff file obtained from Maker was run through agat_convert_sp_gxf2gxf.pl script, which is a part of AGAT tools (60). This step resulted in the removal of 82 identical isoforms and added the missing gene features, leading to a total of 18,196 genes with 29,389 transcripts. Functional annotation was performed by locally blasting the transcripts against a nonredundant (nr) protein database, using diamond blast (61), and a gene ontology analysis was performed using Interproscan in Blast2Go (62). Finally, the blast results were merged with the interproscan results in Blast2Go to produce a final functional annotation for the genome.

Data Availability All raw Illumina reads of RNA-seq, ATAC-seq, and Hi-C are available under NCBI Bioproject PRJNA685019 (<https://dataview.ncbi.nlm.nih.gov/object/PRJNA685019?reviewer=pg4desk3hib1cggbiofrdm7ll>). BaGv2 genome version is available in LepBase (http://ensembl.lepbase.org/Bicyclus_any_nana_bagv2/Info/Index).

ACKNOWLEDGMENTS. We thank the National University of Singapore High Performance Computing for allowing access to perform the bioinformatic analysis and Tirtha Das Banerjee for his comments on the manuscript. This work was supported by the Ministry of Education, Singapore Award MOE2015-T2-2-159 and the National Research Foundation (NRF), Singapore NRF Investigatorship Award NRF-NRFI05-2019-0006 and NRF-CRP20-2017-0001 (to A.M.). S.N.M. was supported by a Yale-NUS scholarship. Y.T. is thankful to the NSF (Grant IOS1557936) and the US Department of Agriculture (Grant 2018-08230).

1. W. J. Glassford et al., Co-option of an ancestral Hox-regulated network underlies a recently evolved morphological novelty. *Dev. Cell* **34**, 520–531 (2015).
2. S. B. Carroll et al., Pattern formation and eyespot determination in butterfly wings. *Science* **265**, 109–114 (1994).
3. S. V. Saenko, V. French, P. M. Brakefield, P. Beldade, Conserved developmental processes and the formation of evolutionary novelties: Examples from butterfly wings. *Philos. Trans. R. Soc. Lond. B Biol. Sci.* **363**, 1549–1555 (2008).
4. L. I. Held, Rethinking butterfly eyespots. *Evol. Biol.* **40**, 158–168 (2013).
5. A. Monteiro, G. Glaser, S. Stockslager, N. Glansdorp, D. Ramos, Comparative insights into questions of lepidopteran wing pattern homology. *BMC Dev. Biol.* **6**, 52 (2006).
6. H. Connahs et al., Activation of butterfly eyespots by Distal-less is consistent with a reaction-diffusion process. *Development* **146**, 1–12 (2019).
7. J. M. Musser, G. P. Wagner, Character trees from transcriptome data: Origin and individuation of morphological characters and the so-called "species signal". *J. Exp. Zool. B Mol. Dev. Evol.* **324**, 588–604 (2015).
8. M. I. Love, W. Huber, S. Anders, Moderated estimation of fold change and dispersion for RNA-seq data with DESeq2. *Genome Biol.* **15**, 550 (2014).
9. R. Suzuki, H. Shimodaira, PvcLust: An R package for assessing the uncertainty in hierarchical clustering. *Bioinformatics* **22**, 1540–1542 (2006).
10. N. Özsu, A. Monteiro, Wound healing, calcium signaling, and other novel pathways are associated with the formation of butterfly eyespots. *BMC Genomics* **18**, 788 (2017).
11. A. Monteiro et al., Distal-less regulates eyespot patterns and melanization in *Bicyclus* butterflies. *J. Exp. Zool. B Mol. Dev. Evol.* **320**, 321–331 (2013).
12. J. D. Uhl, A. Zandvakili, B. Gebelein, A Hox transcription factor collective binds a highly conserved distal-less cis-regulatory module to generate robust transcriptional outcomes. *PLoS Genet.* **12**, e1005981 (2016).
13. J. T. Wagner-Bernholz, O. Wilson, G. Gibson, R. Schuh, W. J. Gehring, Identification of target genes of the homeotic gene Antennapedia by enhancer detection. *Genes Dev.* **6**, 328 (1992).
14. P. D. Dong, J. Chu, G. Panganiban, Coexpression of the homeobox genes Distal-less and homothorax determines *Drosophila* antennal identity. *Development* **127**, 209–216 (2000).
15. J. C. Oliver, X. L. Tong, L. F. Gall, W. H. Piel, A. Monteiro, A single origin for nymphalid butterfly eyespots followed by widespread loss of associated gene expression. *PLoS Genet.* **8**, e1002893 (2012).
16. Y. Matsuoka, A. Monteiro, Hox genes are essential for the development of novel serial homologous eyespots on the wings of *Bicyclus anynana* butterflies. *Genetics* **217**, 1–9 (2020).
17. T. Das Banerjee, A. Monteiro, Molecular mechanisms underlying simplification of venation patterns in holometabolous insects. *Development* **147**, 1–12 (2020).
18. L. Zhang, R. D. Reed, Genome editing in butterflies reveals that spalt promotes and Distal-less represses eyespot colour patterns. *Nat. Commun.* **7**, 11769 (2016).
19. C. R. Brunetti et al., The generation and diversification of butterfly eyespot color patterns. *Curr. Biol.* **11**, 1578–1585 (2001).
20. S. V. Saenko, M. S. P. Marialva, P. Beldade, Involvement of the conserved Hox gene Antennapedia in the development and evolution of a novel trait. *Evodevo* **2**, 9 (2011).
21. G. Panganiban, Distal-less function during *Drosophila* appendage and sense organ development. *Dev. Dyn.* **218**, 554–562 (2000).
22. B. S. Emerald, S. M. Cohen, Spatial and temporal regulation of the homeotic selector gene Antennapedia is required for the establishment of leg identity in *Drosophila*. *Dev. Biol.* **267**, 462–472 (2004).
23. A. Monteiro, O. Podlaha, Wings, horns, and butterfly eyespots: How do complex traits evolve? *PLoS Biol.* **7**, e37 (2009).
24. Y. T. Lai, et al., Enhancer identification and activity evaluation in the red flour beetle, *Tribolium castaneum*. *Development* **145**, 1–13 (2018).
25. G. Panganiban, J. L. R. Rubenstein, Developmental functions of the Distal-less/Dlx homeobox genes. *Development* **129**, 4371–4386 (2002).
26. H. S. Bruce, N. H. Patel, Knockout of crustacean leg patterning genes suggests that insect wings and body walls evolved from ancient leg segments. *Nat. Ecol. Evol.* **4**, 1703–1712 (2020).
27. C. M. Clark-Hachtel, Y. Tomoyasu, Two sets of candidate crustacean wing homologues and their implication for the origin of insect wings. *Nat. Ecol. Evol.* **4**, 1694–1702 (2020).
28. G. Sabaris, I. Laiker, E. Preger-Ben Noon, N. Frankel, Actors with multiple roles: Pleiotropic enhancers and the paradigm of enhancer modularity. *Trends Genet.* **35**, 423–433 (2019).
29. B. Prud'homme, N. Gompel, S. B. Carroll, Emerging principles of regulatory evolution. *Proc. Natl. Acad. Sci. U.S.A.* **104** (suppl. 1), 8605–8612 (2007).
30. H. Li, R. Durbin, Fast and accurate short read alignment with Burrows-Wheeler transform. *Bioinformatics* **25**, 1754–1760 (2009).
31. H. Li et al.; 1000 Genome Project Data Processing Subgroup, The sequence alignment/map format and SAMtools. *Bioinformatics* **25**, 2078–2079 (2009).
32. A. R. Quinlan, I. M. Hall, BEDTools: A flexible suite of utilities for comparing genomic features. *Bioinformatics* **26**, 841–842 (2010).
33. Y. Zhang et al., Model-based analysis of ChIP-Seq (MACS). *Genome Biol.* **9**, R137 (2008).
34. Y. Naito, K. Hino, H. Bono, K. Ui-Tei, CRISPRdirect: Software for designing CRISPR/Cas guide RNA with reduced off-target sites. *Bioinformatics* **31**, 1120–1123 (2015).
35. K. N. Eckeremann et al., Hyperactive piggyBac transposase improves transformation efficiency in diverse insect species. *Insect Biochem. Mol. Biol.* **98**, 16–24 (2018).

36. C. J. Evans *et al.*, G-TRACE: Rapid Gal4-based cell lineage analysis in *Drosophila*. *Nat. Methods* **6**, 603–605 (2009).
37. J. F. de Celis, R. Barrio, F. C. Kafatos, Regulation of the spalt/spalt-related gene complex and its function during sensory organ development in the *Drosophila thorax*. *Development* **126**, 2653–2662 (1999).
38. P. S. Aranda, D. M. LaJoie, C. L. Jorczyk, Bleach gel: A simple agarose gel for analyzing RNA quality. *Electrophoresis* **33**, 366–369 (2012).
39. B. Bushnell, BMAP: A Fast, Accurate, Splice-Aware Aligner. <https://sourceforge.net/projects/bbmap/> (Accessed 19 November 2020).
40. E. Kopylova, L. Noé, H. Touzet, SortMeRNA: Fast and accurate filtering of ribosomal RNAs in metatranscriptomic data. *Bioinformatics* **28**, 3211–3217 (2012).
41. M. Perte, D. Kim, G. M. Perte, J. T. Leek, S. L. Salzberg, Transcript-level expression analysis of RNA-seq experiments with HISAT, StringTie and Ballgown. *Nat. Protoc.* **11**, 1650–1667 (2016).
42. M. S. Campbell, C. Holt, B. Moore, M. Yandell, *Genome Annotation and Curation Using MAKER and MAKER-P*. *Curr. Protoc. Bioinformatics* **48**, 48.4.11.1–39 (2014).
43. B. J. Haas, *et al.*, *De novo transcript sequence reconstruction from RNA-Seq: reference generation and analysis with Trinity*. *Nat. Protoc.* **8**, 1494–1512 (2013).
44. C. R. Fisher, J. L. Wegrzyn, E. L. Jockusch, Co-option of wing-patterning genes underlies the evolution of the treehopper helmet. *Nat. Ecol. Evol.* **4**, 250–260 (2020).
45. R Core Team, *R: A Language and Environment for Statistical Computing* (R Foundation for Statistical Computing, Vienna, Austria, 2020). <https://www.R-project.org/>. Accessed 1 March 2021.
46. T. Wei, V. Simko, R. Package ‘corrplot’: Visualization of a Correlation Matrix. (Version 0.92). <https://github.com/taiyun/corrplot>. Accessed 10 February 2022.
47. M. R. Corces *et al.*, An improved ATAC-seq protocol reduces background and enables interrogation of frozen tissues. *Nat. Methods* **14**, 959–962 (2017).
48. J. J. Lewis *et al.*, Parallel evolution of ancient, pleiotropic enhancers underlies butterfly wing pattern mimicry. *Proc. Natl. Acad. Sci. U.S.A.* **116**, 24174–24183 (2019).
49. J. J. Lewis, R. D. Reed, Genome-wide regulatory adaptation shapes population-level genomic landscapes in *Heliconius*. *Mol. Biol. Evol.* **36**, 159–173 (2019).
50. A. P. Boyle, J. Guinney, G. E. Crawford, T. S. Furey, F-Seq: A feature density estimator for high-throughput sequence tags. *Bioinformatics* **24**, 2537–2538 (2008).
51. Y. Liao, G. K. Smyth, W. Shi, featureCounts: An efficient general purpose program for assigning sequence reads to genomic features. *Bioinformatics* **30**, 923–930 (2014).
52. F. Ramírez, F. Dündar, S. Diehl, B. A. Grüning, T. Manke, deepTools: A flexible platform for exploring deep-sequencing data. *Nucleic Acids Res.* **42**, W187–91 (2014).
53. N. C. Durand *et al.*, Juicer provides a one-click system for analyzing loop-resolution Hi-C experiments. *Cell Syst.* **3**, 95–98 (2016).
54. J. Ray *et al.*, Chromatin conformation remains stable upon extensive transcriptional changes driven by heat shock. *Proc. Natl. Acad. Sci. U.S.A.* **116**, 19431–19439 (2019).
55. R. W. Nowell *et al.*, A high-coverage draft genome of the mycalesine butterfly *Bicyclus anynana*. *Gigascience* **6**, 1–7 (2017).
56. P. Beldade, S. V. Saenko, N. Pul, A. D. Long, A gene-based linkage map for *Bicyclus anynana* butterflies allows for a comprehensive analysis of synteny with the lepidopteran reference genome. *PLoS Genet.* **5**, e1000366 (2009).
57. J. Catchen, A. Amores, S. Bassham, Chromonomer: A tool set for repairing and enhancing assembled genomes through integration of genetic maps and conserved synteny. *G3 (Bethesda)* **10**, 10.1534/g3.120.401485 (2020).
58. F. A. Simão, R. M. Waterhouse, P. Ioannidis, E. V. Kriventseva, E. M. Zdobnov, BUSCO: Assessing genome assembly and annotation completeness with single-copy orthologs. *Bioinformatics* **31**, 3210–3212 (2015).
59. P. Jones *et al.*, InterProScan 5: Genome-scale protein function classification. *Bioinformatics* **30**, 1236–1240 (2014).
60. J. Dainat, AGAT: Another Gff Analysis Toolkit to handle annotations in any GTF/GFF format. (Version v0.4.0) (2020) 10.5281/ZENODO.4205393. Accessed 19 November 2020.
61. B. Buchfink, C. Xie, D. H. Huson, Fast and sensitive protein alignment using DIAMOND. *Nat. Methods* **12**, 59–60 (2015).
62. S. Götz *et al.*, High-throughput functional annotation and data mining with the Blast2GO suite. *Nucleic Acids Res.* **36**, 3420–3435 (2008).